

FIG. 1A

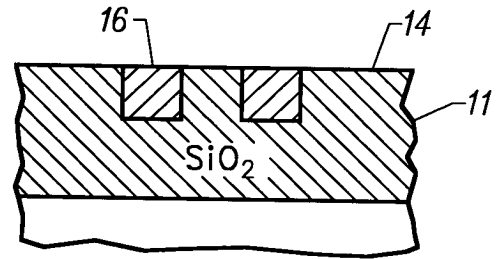


FIG. 1B

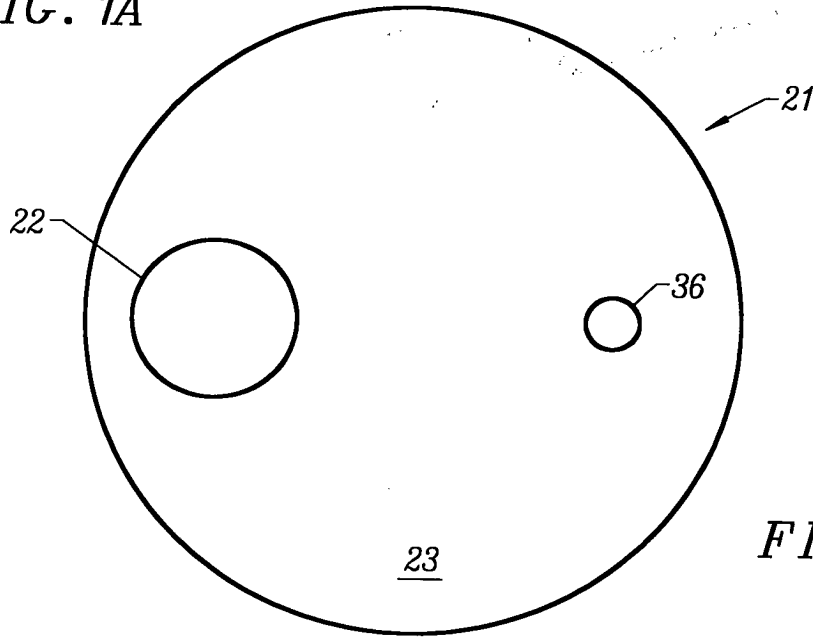


FIG. 2

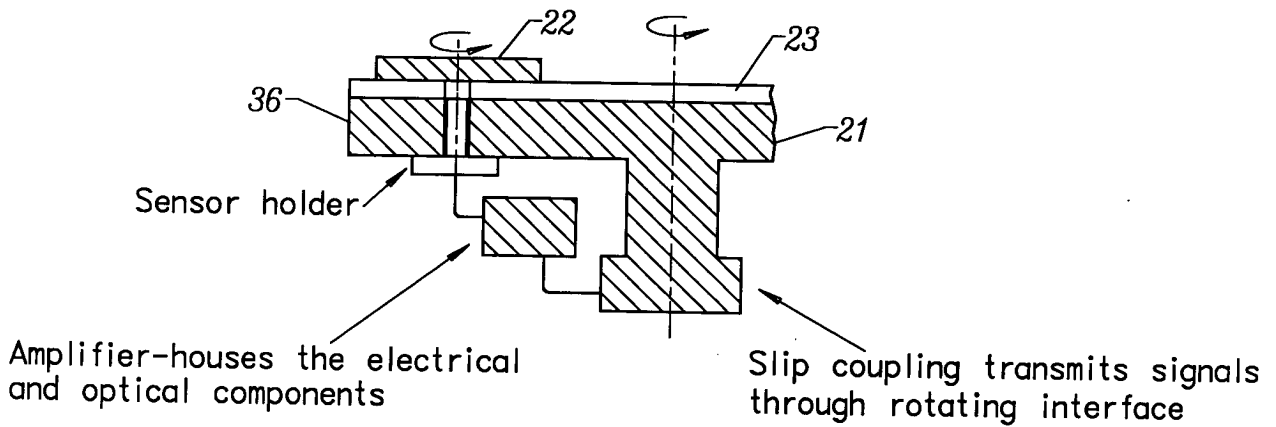


FIG. 3

10029080 12101

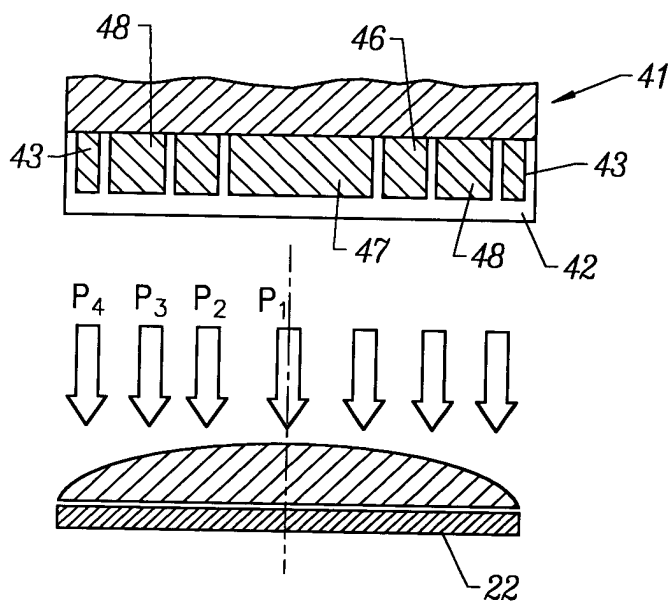


FIG. 4

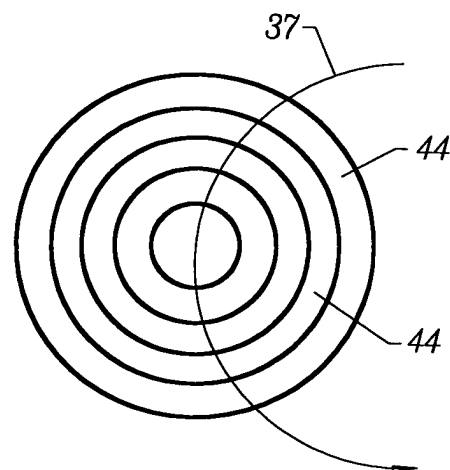


FIG. 5

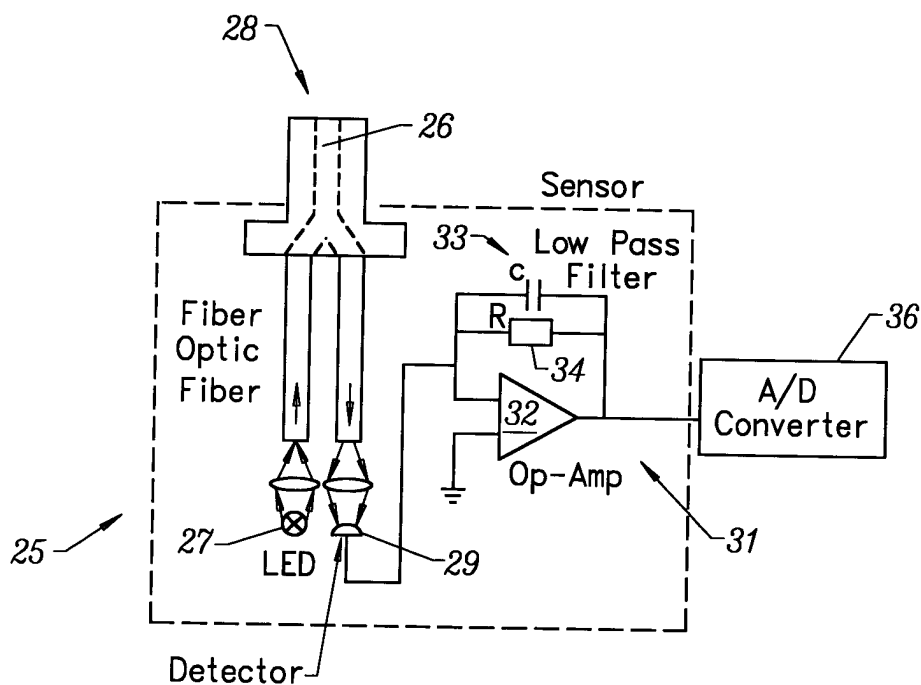


FIG. 6

10029080-12101

3/29

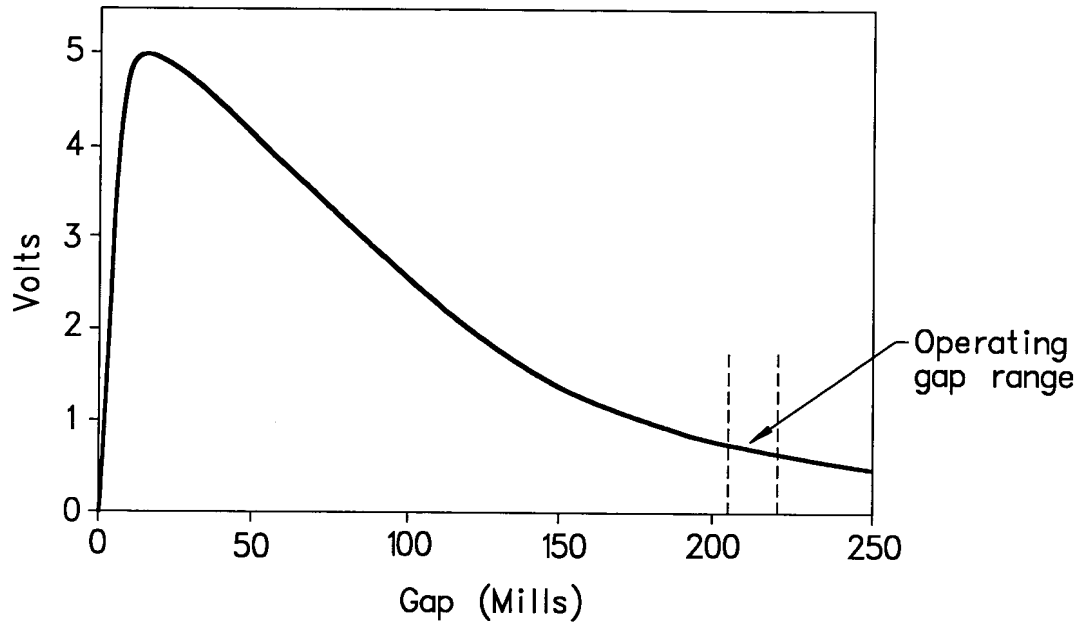


FIG. 7

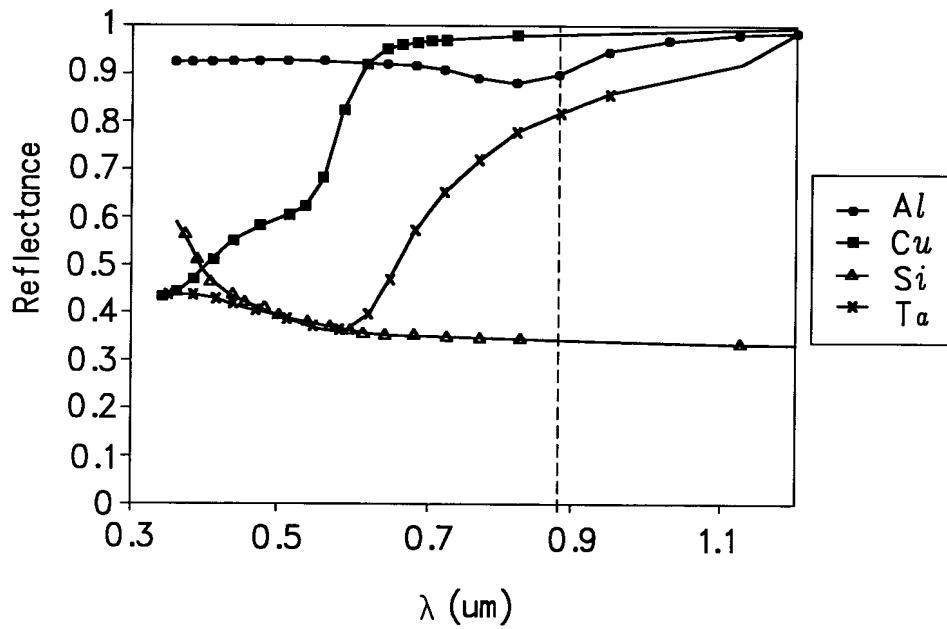


FIG. 8

4/29

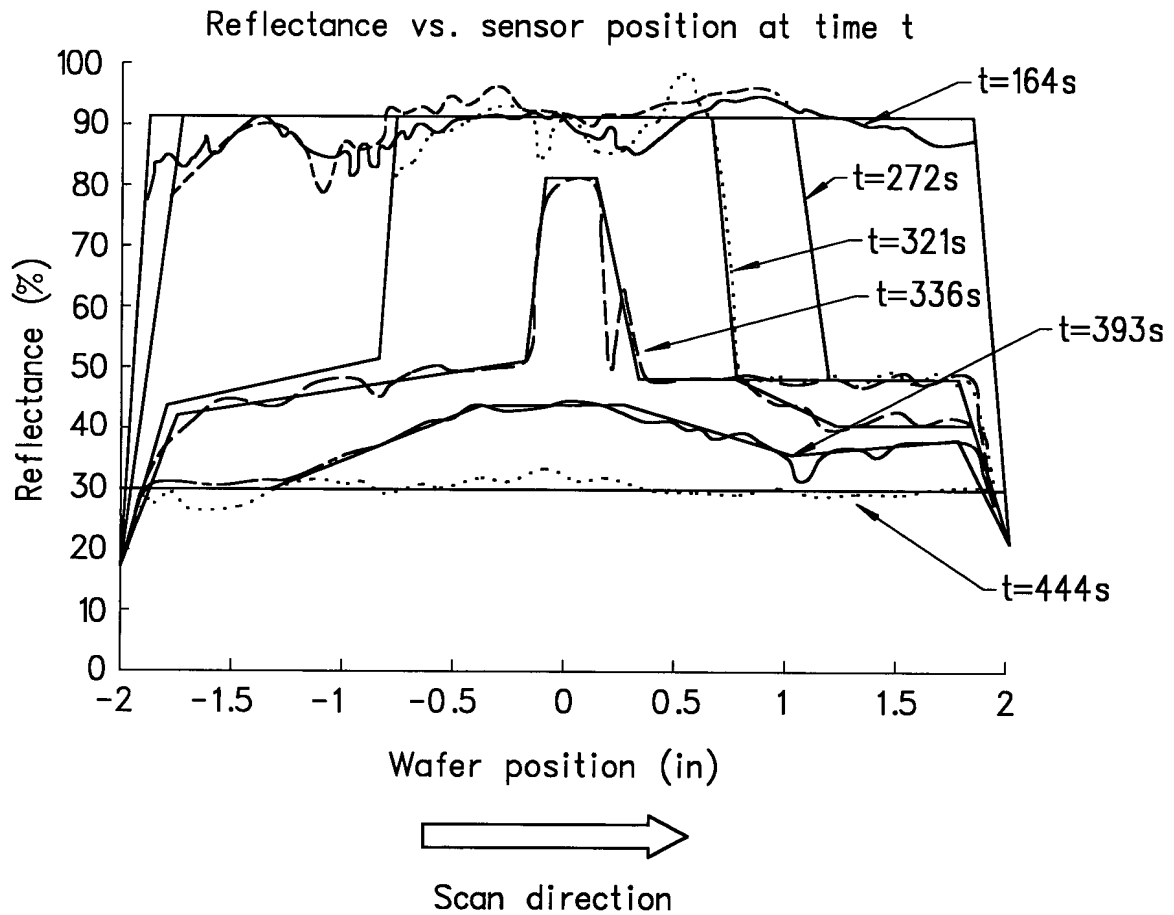


FIG. 9

5/29

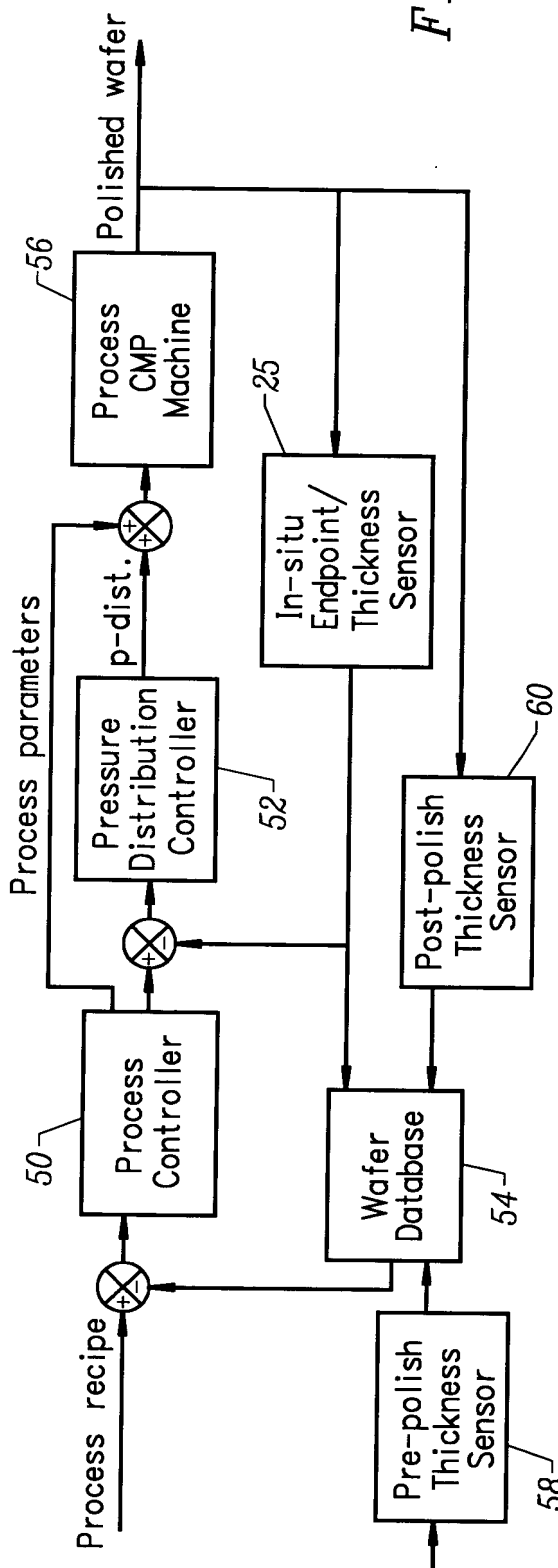


FIG. 11

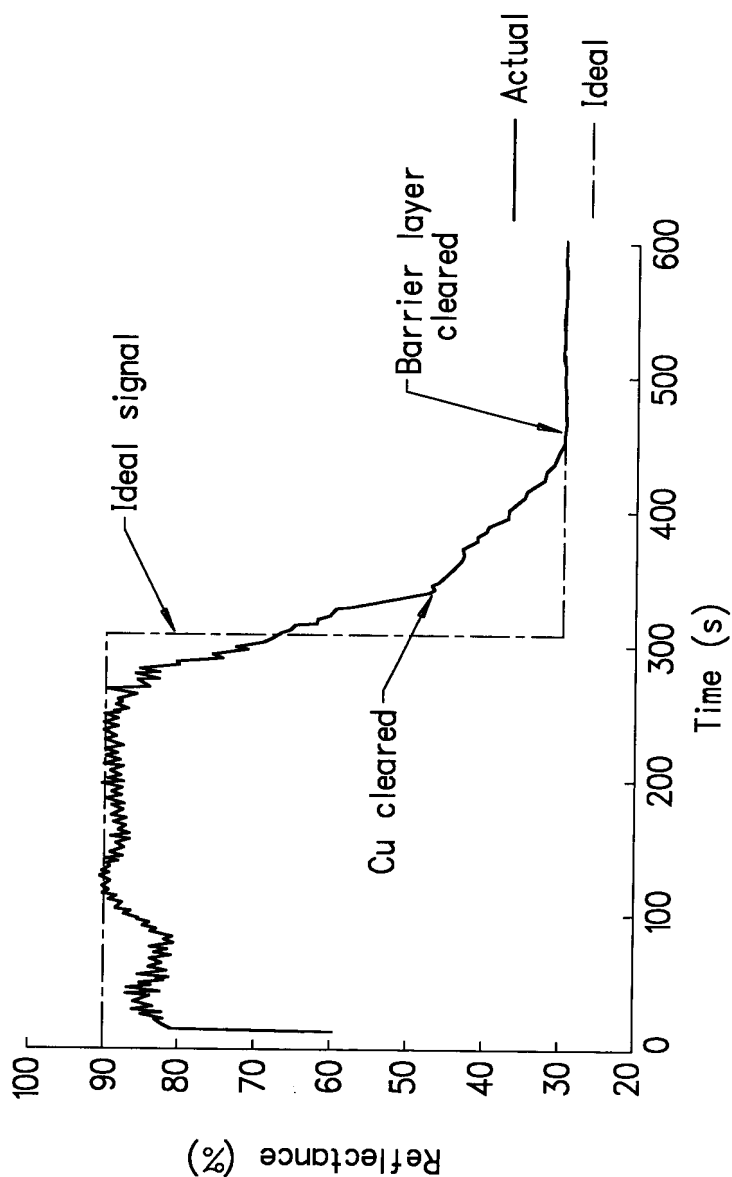


FIG. 10

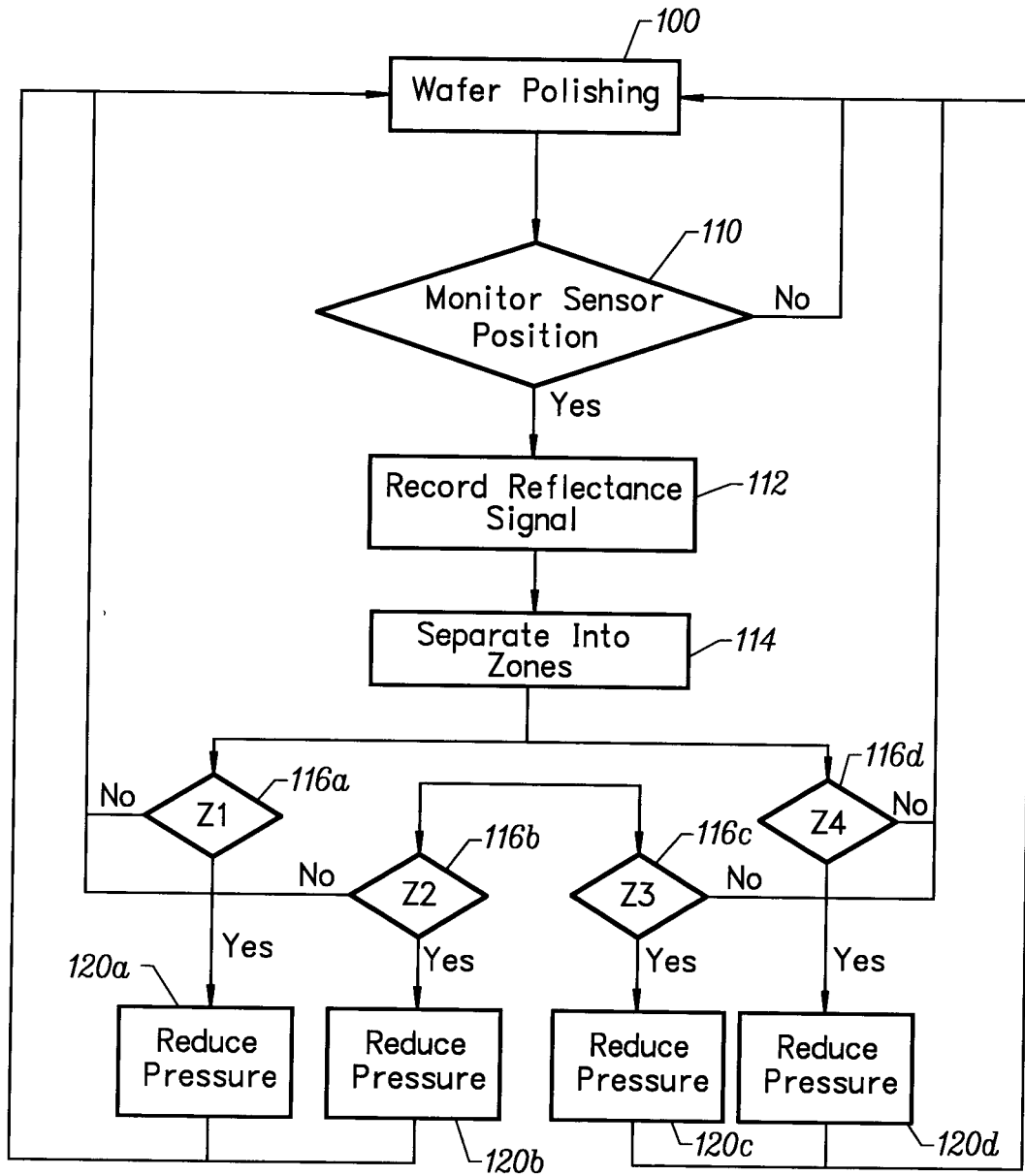


FIG. 12

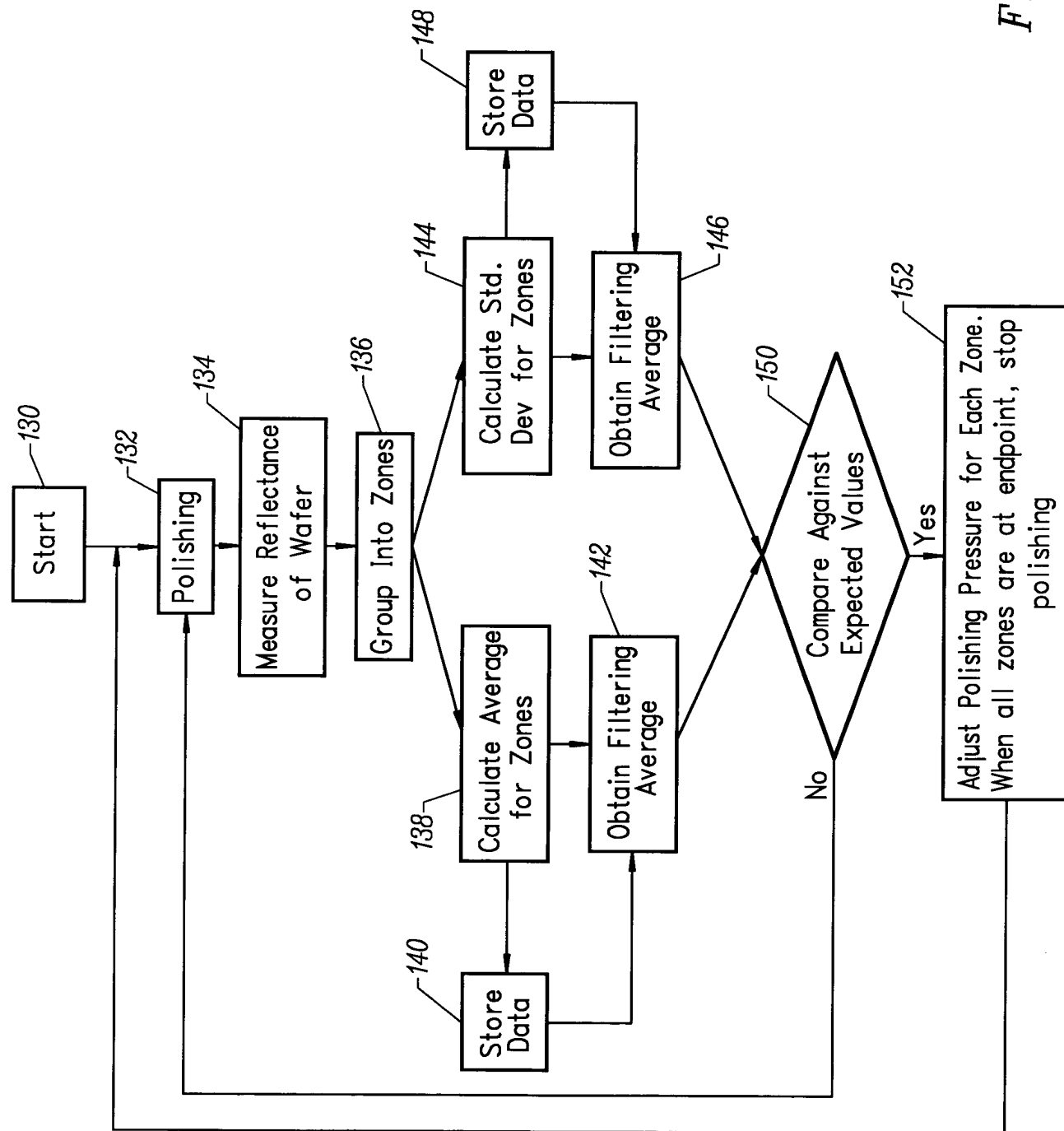
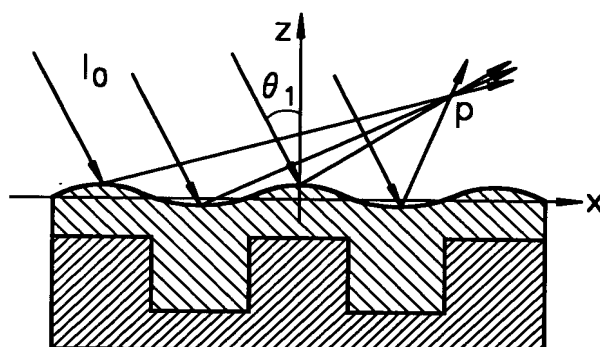


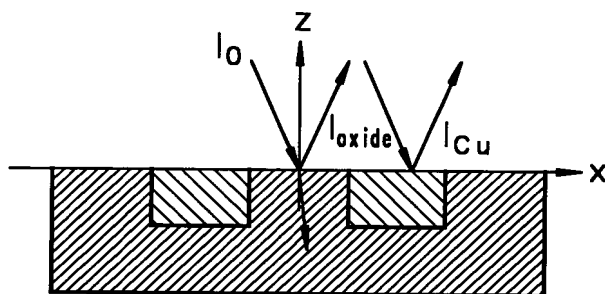
FIG. 13

8/29



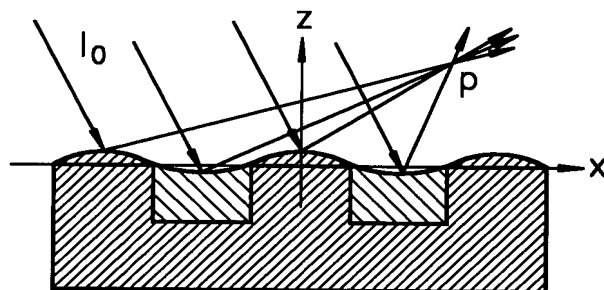
Schematics of light scattering on a patterned Cu surface.

FIG. 14



Schematics of light scattering from a planar composite surface.

FIG. 15A

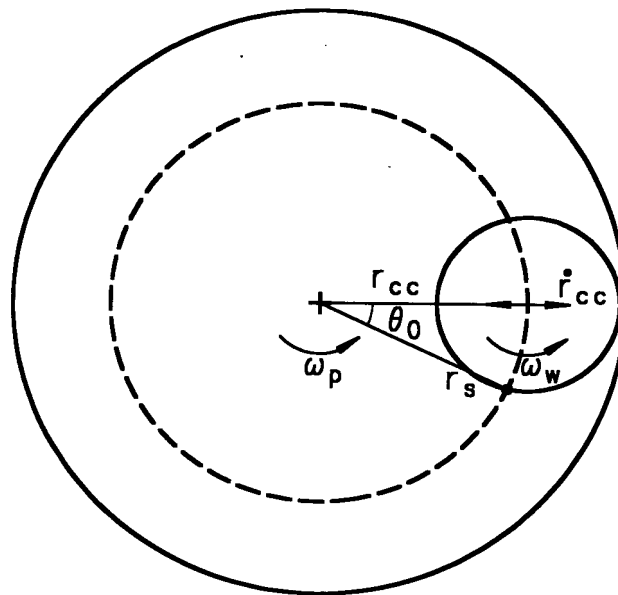


Schematics of light scattering from a wavy composite surface.

FIG. 15B

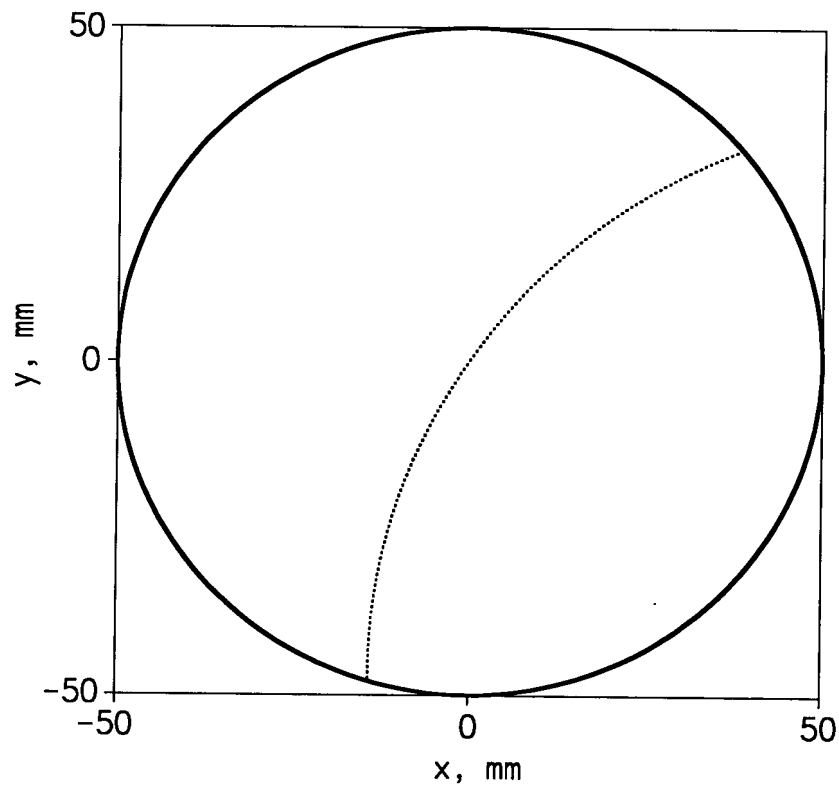
10029080 122101

9/29



Sensor kinematics.

FIG. 16

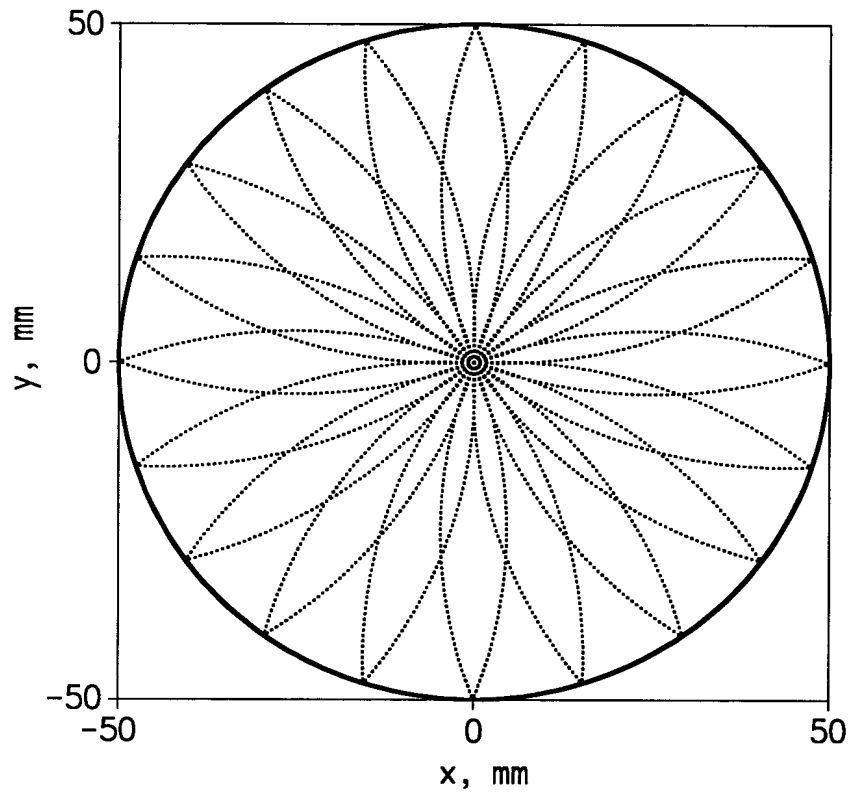


The simulated locus for the reflectance sensor across the wafer at the condition $\omega_w = \omega_p$ and $r_s = r_{cc}$.

FIG. 17

10029080-122101

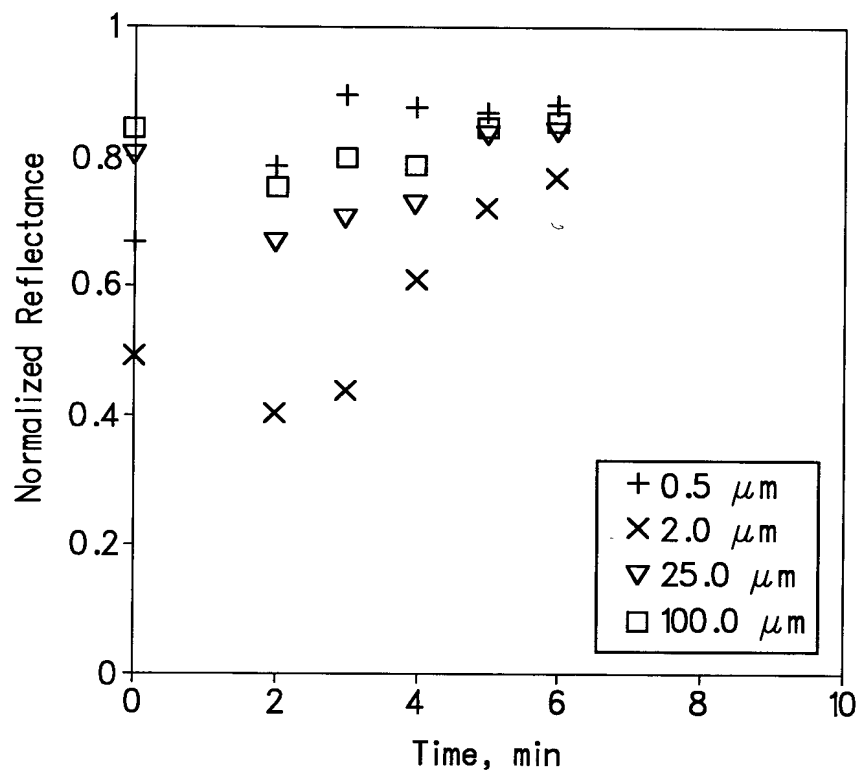
10/29



The simulated locus for the reflectance sensor across the wafer at the condition $\omega_w = 1.05\omega_p$ and $r_s = r_{cc}$.

FIG. 18

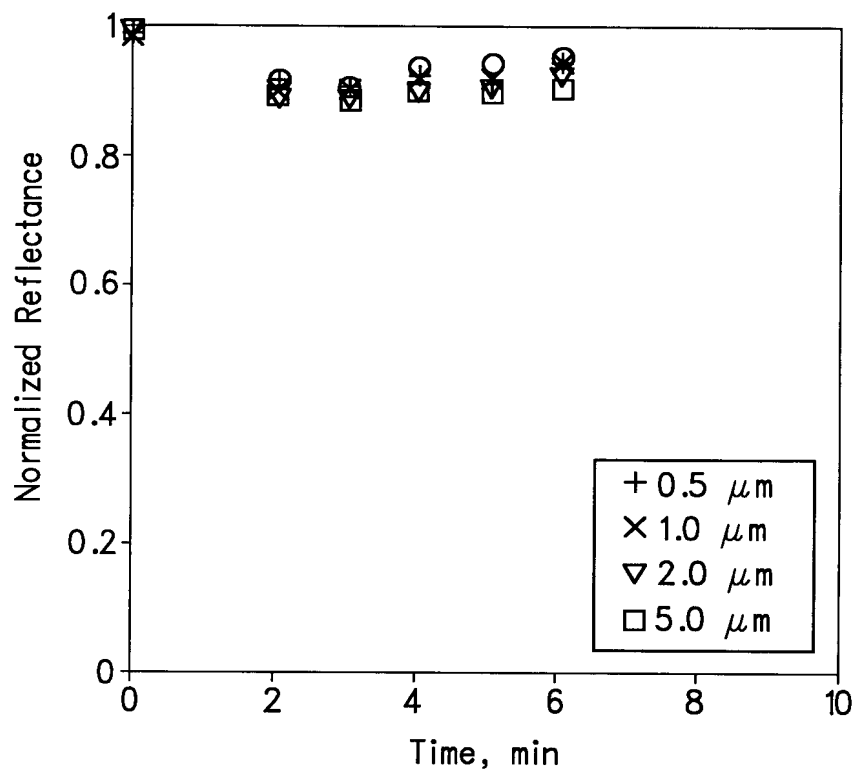
11/29



The results of off-line measurements at the Cu Planarization regimes on the pattern with 0.5 area fraction ($\omega/\lambda = 0.5$).

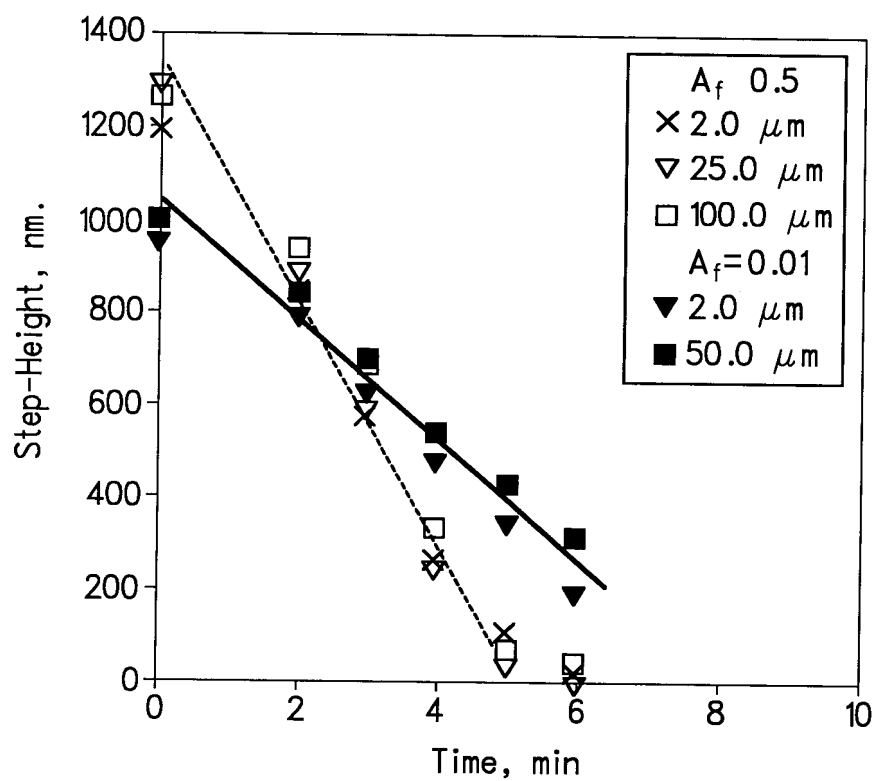
FIG. 19

12/29



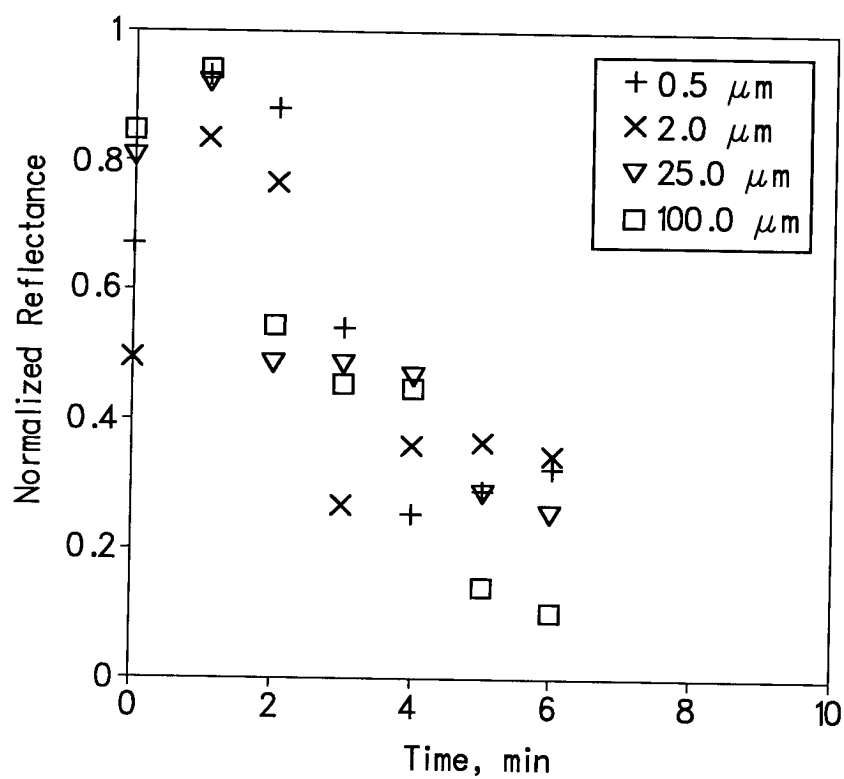
The results of off-line measurements at the Cu Planarization regimes on the patterns with 0.01 area fraction ($\omega/\lambda = 0.1$).

FIG. 20



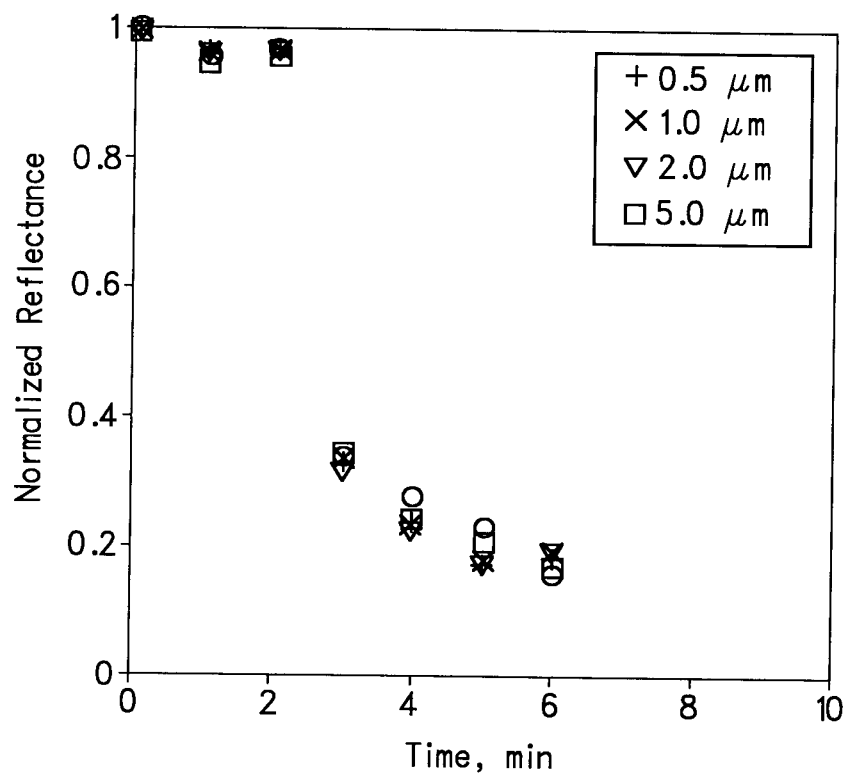
Time evolution of step-heights for patterns with constant area fraction 0.5 and 0.01.

FIG. 21



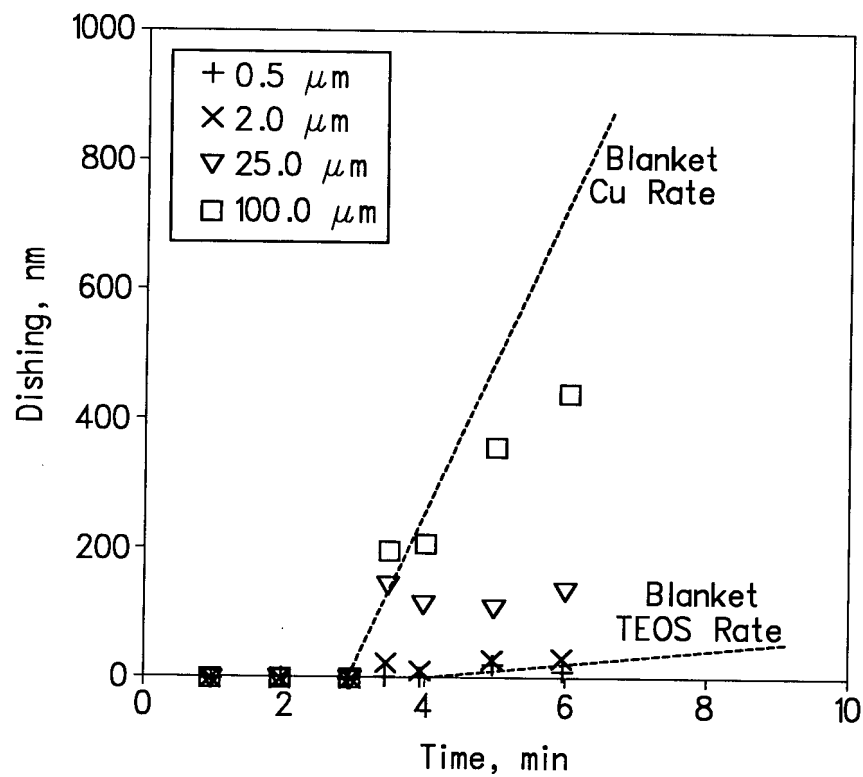
The results of off-line measurements at various process regimes on the pattern with 0.5 area fraction.

FIG. 22



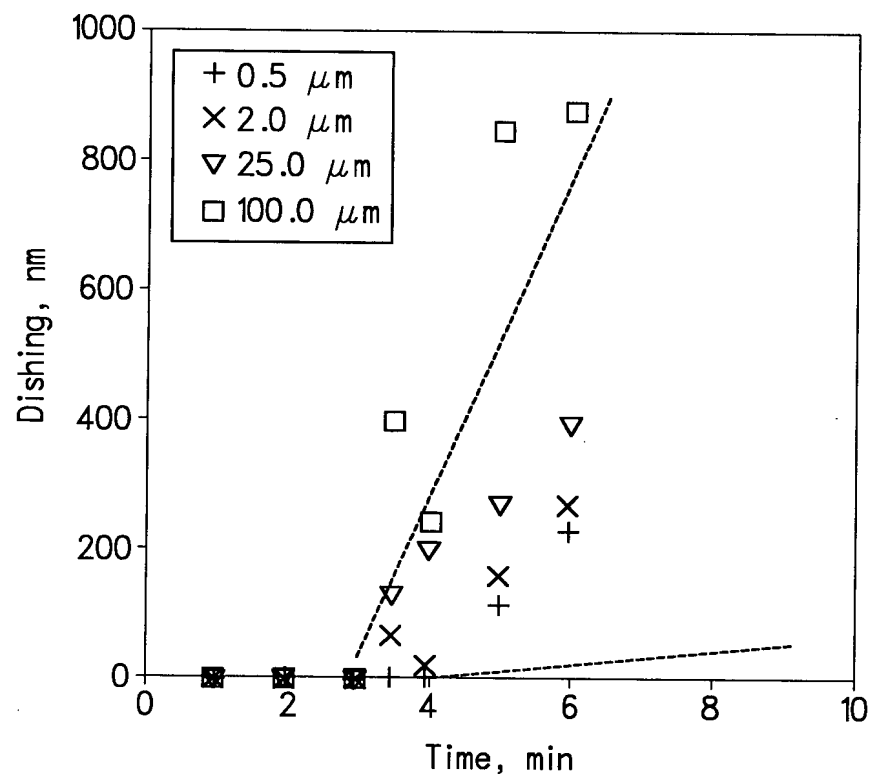
The results of off-line measurements at various process regimes on the pattern with 0.01 area fraction.

FIG. 23



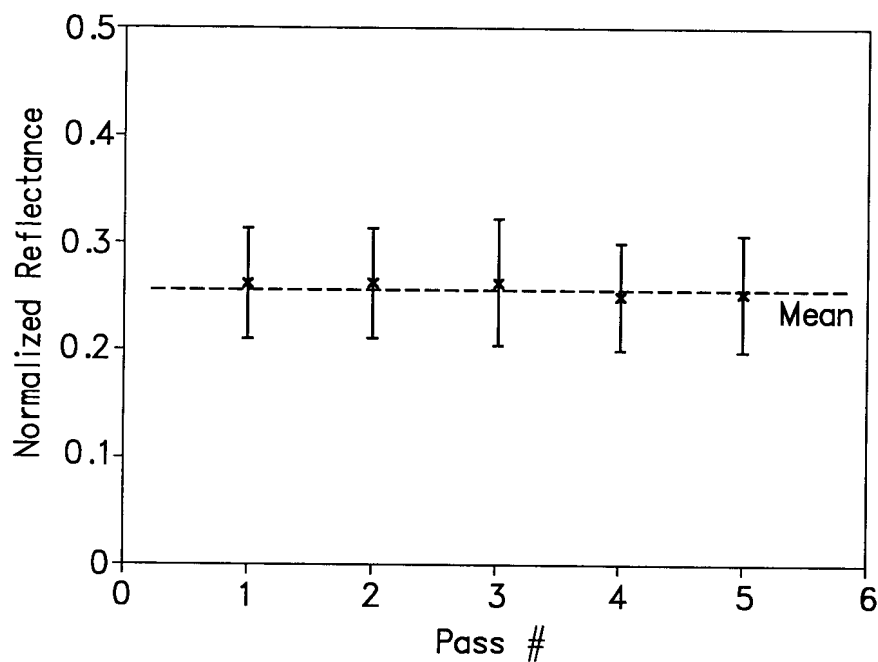
Time evolution of Cu dishing for patterns with constant area fraction 0.5 and various linewidths.

FIG. 24



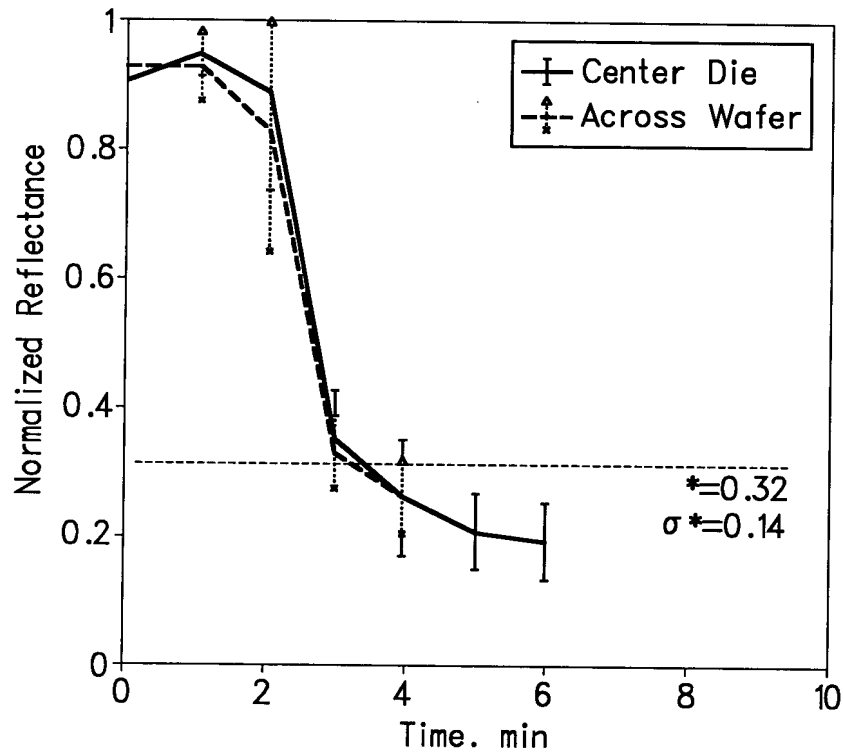
Time evolution of Cu dishing for patterns with constant area fraction 0.01 and various linewidths.

FIG. 25



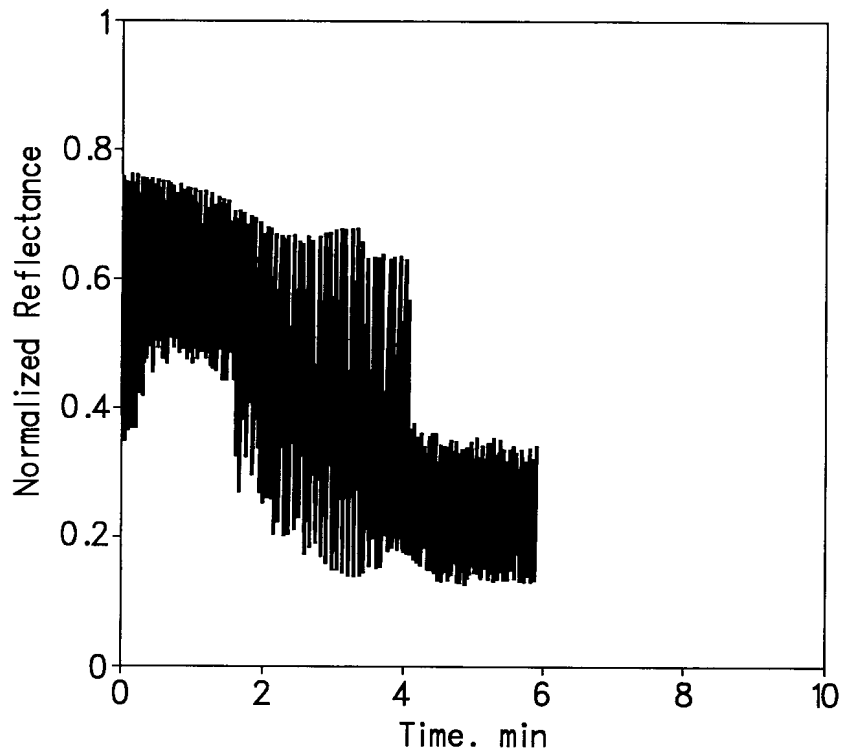
Off-line measurements of the mean and standard deviation of surface reflectance along different loci across the wafer at the onset of endpoint.

FIG. 26



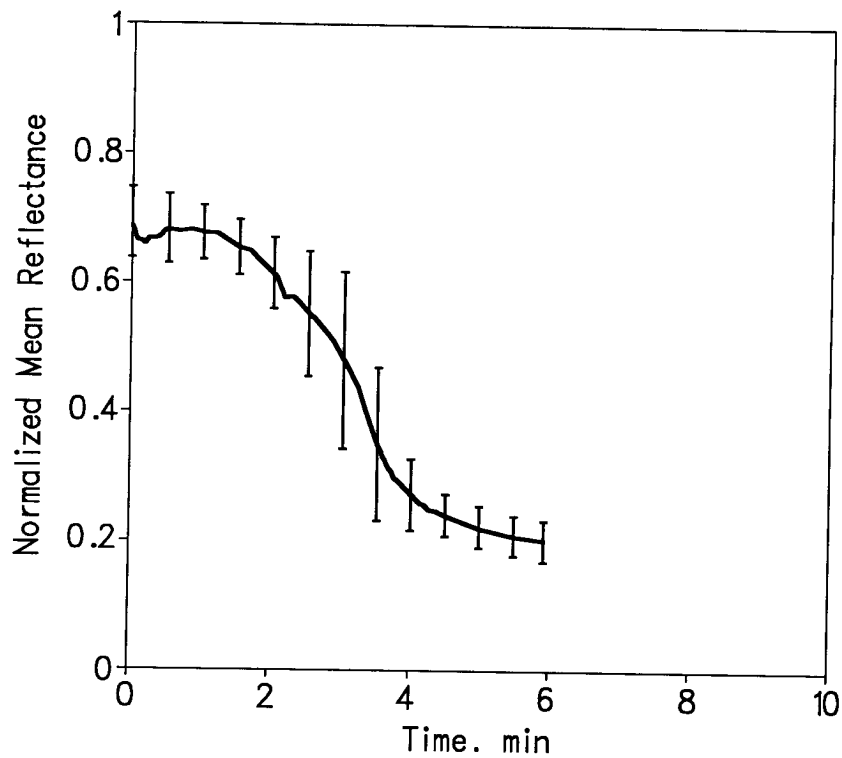
Comparison of the off-line measurements (mean and standard deviation) on the center die and across wafer at various polishing stages. The across-wafer data is calculated based on the measurements along five loci.

FIG. 27



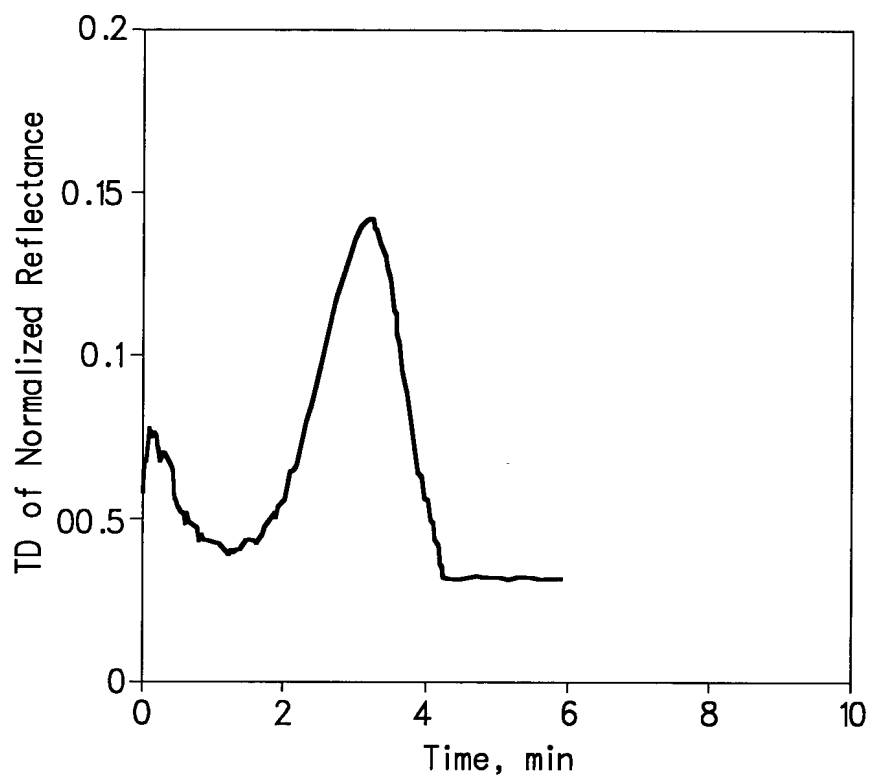
Raw data from in-situ reflectance measurement.

FIG. 28



Results of in-situ measurements of the moving average and standard deviation of wafer-level surface reflectance.

FIG. 29



Results of in-situ measurements of the standard deviation of wafer-level surface reflectance.

FIG. 30

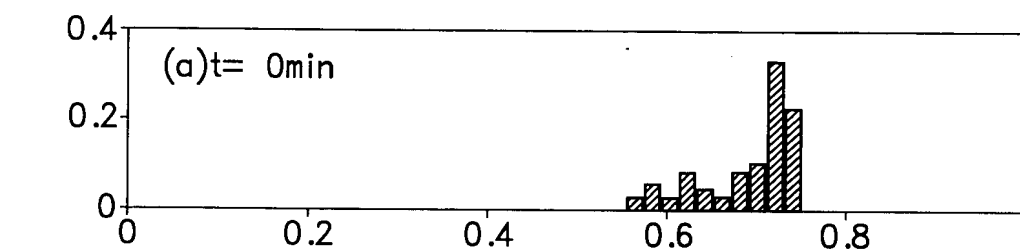


FIG. 31A

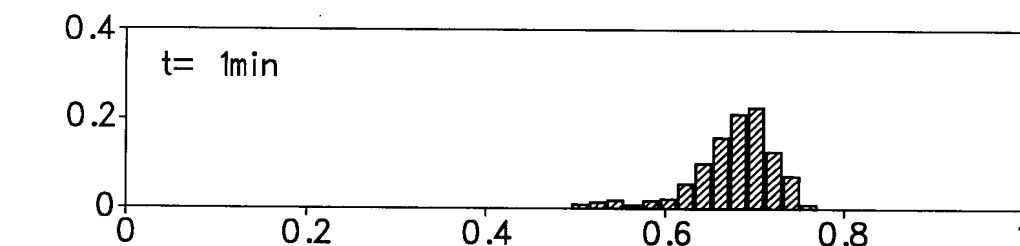


FIG. 31B

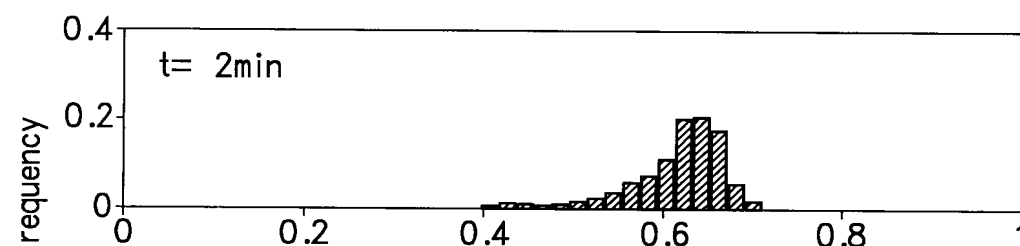


FIG. 31C

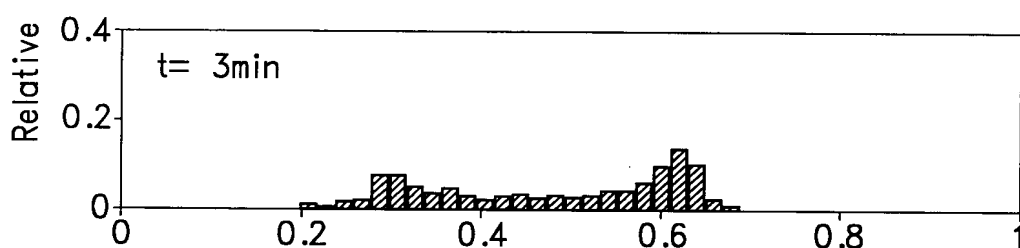


FIG. 31D

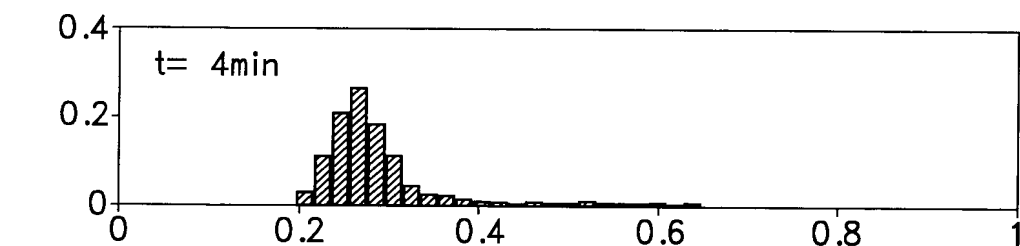


FIG. 31E

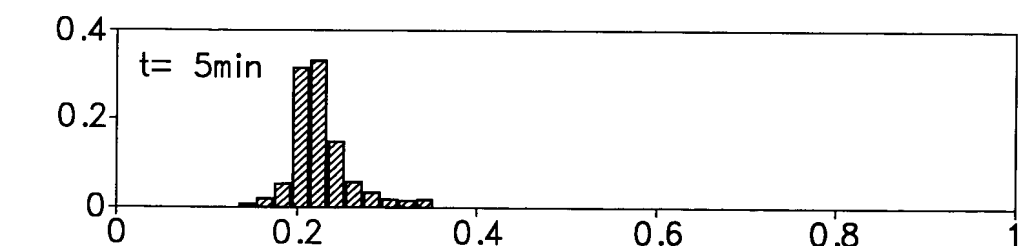
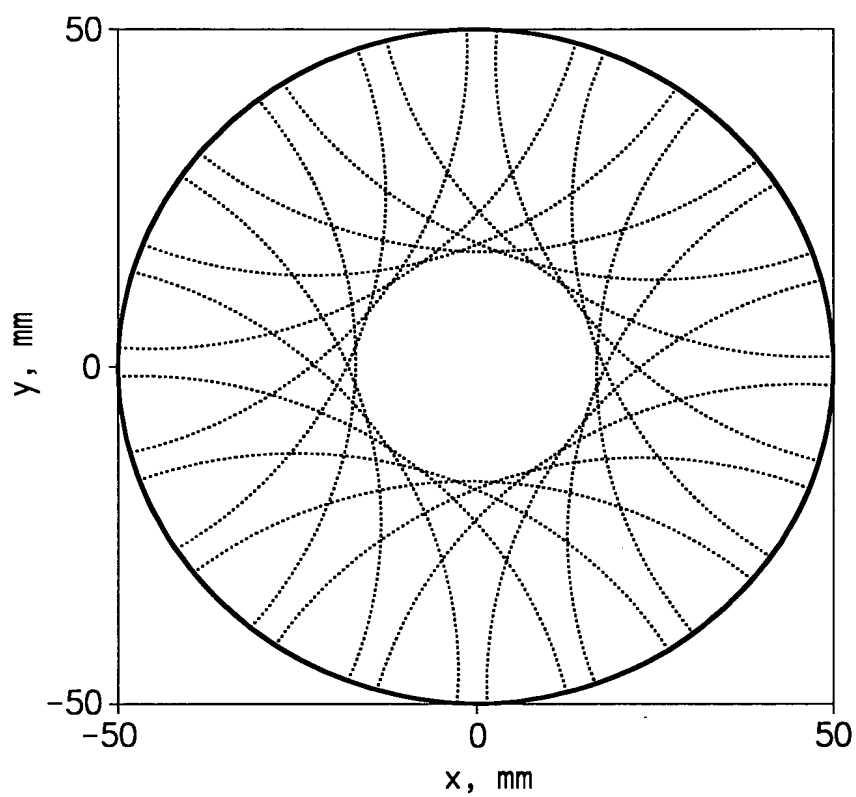


FIG. 31F

Normalized Reflectance

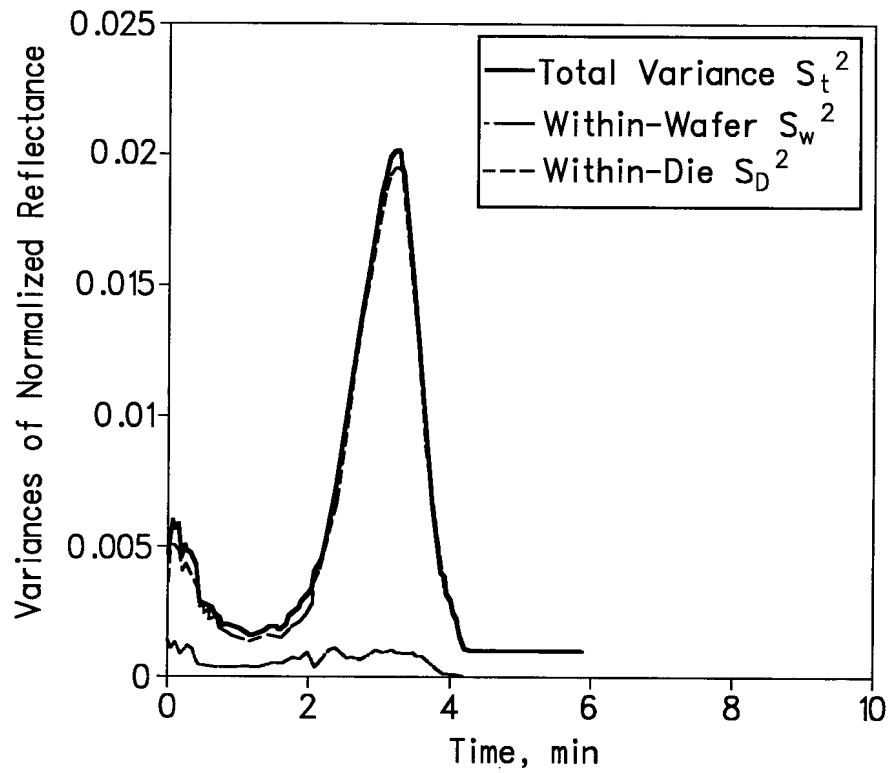
Distribution of surface reflectance versus polishing time from the in-situ measurements.

Downloaded from ascelibrary.org by University of California, San Diego on 06/06/14



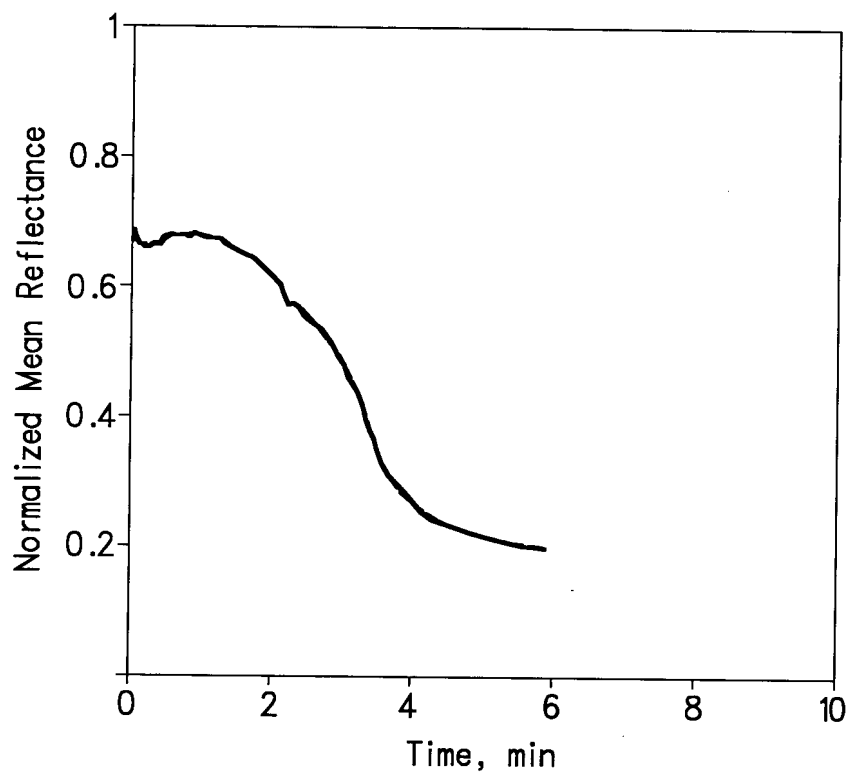
The simulated loci for the reflectance sensor across the wafer at the condition $1.05\omega_w = \omega_p$ and $r_s = 1.25r_{cc}$.

FIG. 32



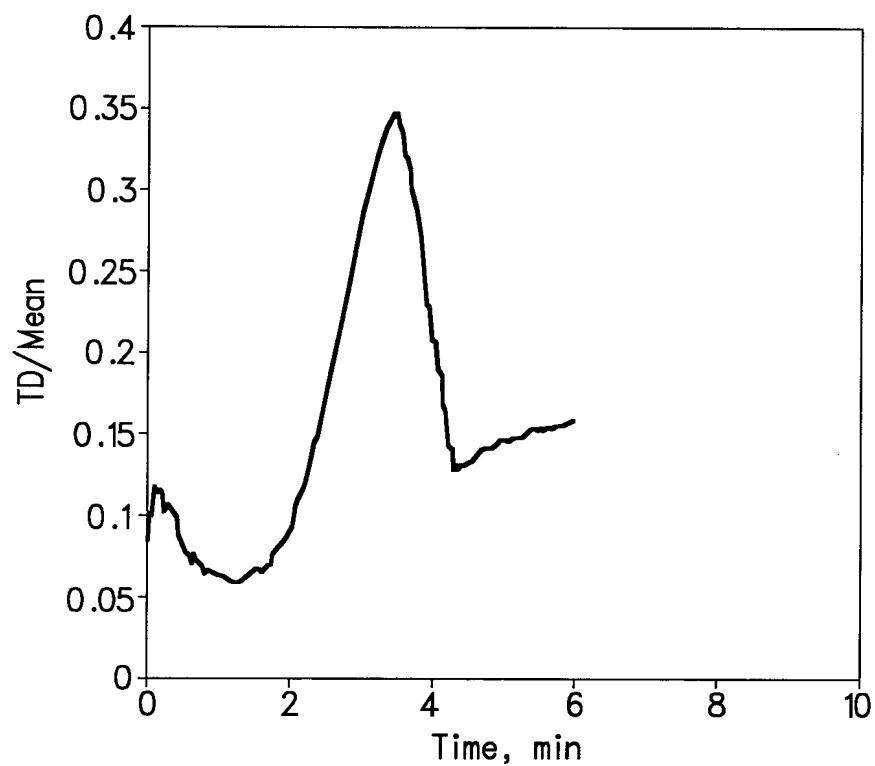
Decomposition of the within-wafer and within-die variance for the in-situ measurements.

FIG. 33



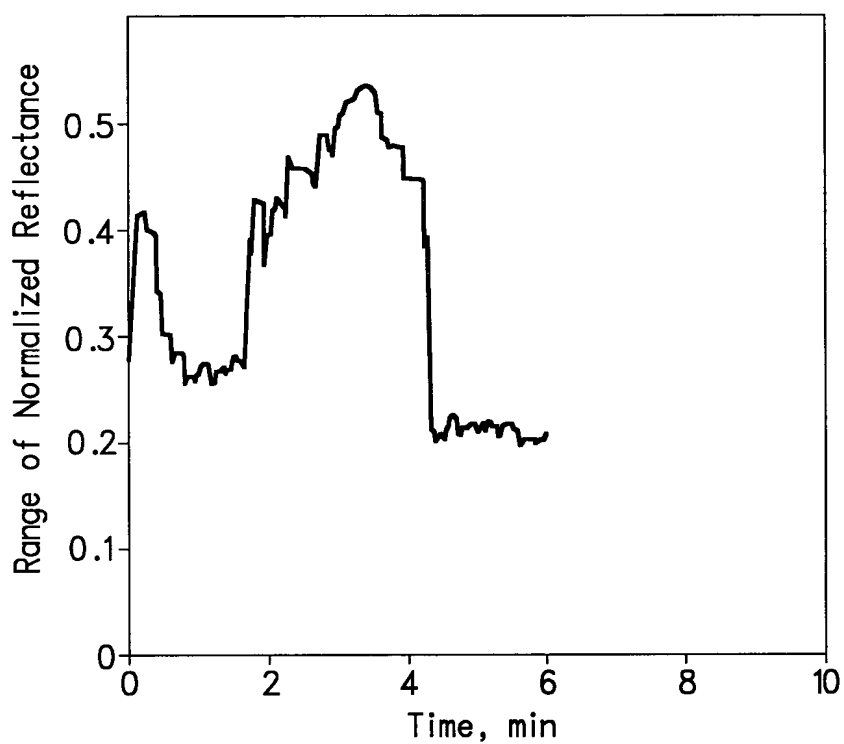
Results of the moving average versus time
with estimated interval at 99.5% confidence interval.

FIG. 34



Results of in-situ measurements of the standard deviation to the mean reflectance (wafer-level).

FIG. 35



Results of the range of surface reflectance versus polishing time (wafer-level).

FIG. 36

29/29

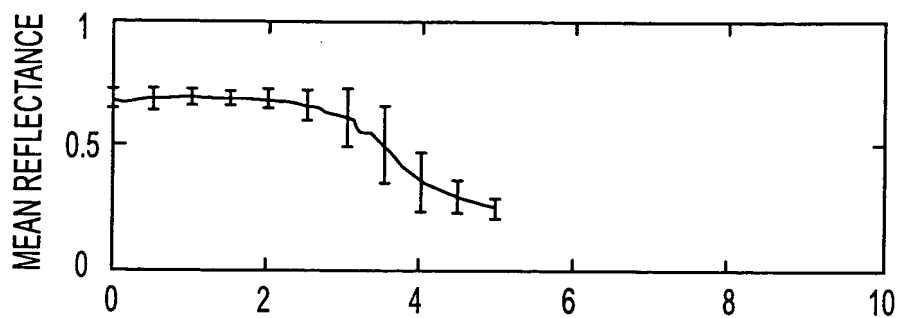


FIG. 37A

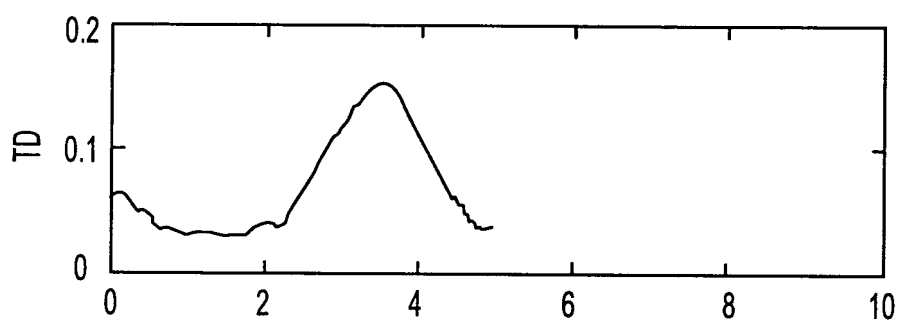


FIG. 37B

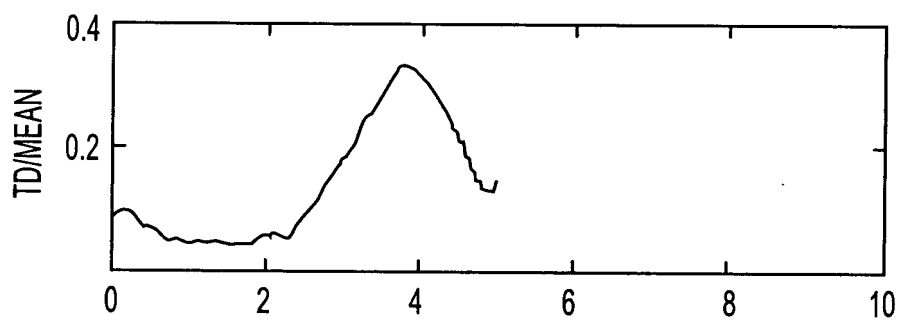


FIG. 37C

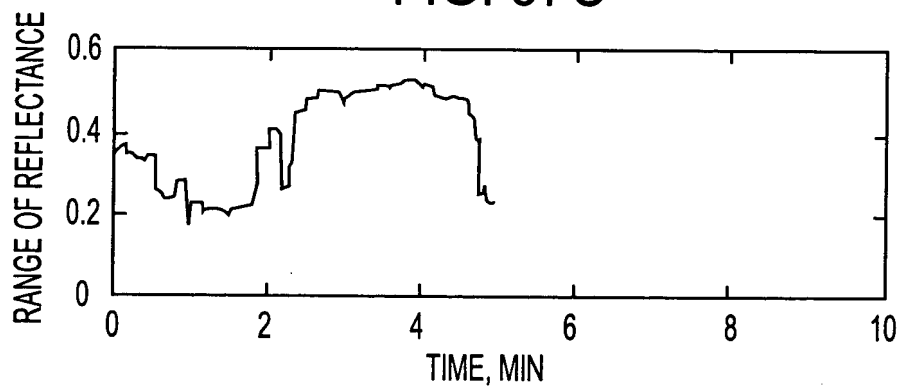


FIG. 37D

TOP SECRET